

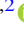





GW190521: Orbital Eccentricity and Signatures of Dynamical Formation in a Binary Black Hole Merger Signal

Isobel Romero-Shaw^{1,2} , Paul D. Lasky^{1,2} , Eric Thrane^{1,2} , and Juan Calderón Bustillo^{1,2,3,4} 

¹School of Physics and Astronomy, Monash University, Clayton, VIC 3800, Australia; isobel.romero-shaw@monash.edu

²OzGrav: The ARC Centre of Excellence for Gravitational Wave Discovery, Clayton, VIC 3800, Australia

³Department of Physics, The Chinese University of Hong Kong, Shatin, N.T., Hong Kong

⁴Instituto Galego de Física de Altas Enerxías, Universidade de Santiago de Compostela, 15782 Santiago de Compostela, Galicia, Spain

Received 2020 September 11; revised 2020 September 29; accepted 2020 October 5; published 2020 October 23

Abstract

Pair-instability supernovae are thought to restrict the formation of black holes in the mass range $\sim 50\text{--}135 M_{\odot}$. However, black holes with masses within this “high mass gap” are expected to form as the remnants of binary black hole mergers. These remnants can merge again dynamically in densely populated environments such as globular clusters. The hypothesis that the binary black hole merger GW190521 formed dynamically is supported by its high mass. Orbital eccentricity can also be a signature of dynamical formation, since a binary that merges quickly after becoming bound may not circularize before merger. In this work, we measure the orbital eccentricity of GW190521. We find that the data prefer a signal with eccentricity $e \geq 0.1$ at 10 Hz to a nonprecessing, quasi-circular signal, with a log Bayes factor $\ln \mathcal{B} = 5.0$. When compared to precessing, quasi-circular analyses, the data prefer a nonprecessing, $e \geq 0.1$ signal, with log Bayes factors $\ln \mathcal{B} \approx 2$. Using injection studies, we find that a nonspinning, moderately eccentric ($e = 0.13$) GW190521-like binary can be mistaken for a quasi-circular, precessing binary. Conversely, a quasi-circular binary with spin-induced precession may be mistaken for an eccentric binary. We therefore cannot confidently determine whether GW190521 was precessing or eccentric. Nevertheless, since both of these properties support the dynamical formation hypothesis, our findings support the hypothesis that GW190521 formed dynamically.

Unified Astronomy Thesaurus concepts: [Black holes \(162\)](#); [Compact objects \(288\)](#); [High energy astrophysics \(739\)](#); [Dynamical evolution \(421\)](#); [Eccentricity \(441\)](#); [Gravitational wave astronomy \(675\)](#); [Gravitational waves \(678\)](#); [Gravitational wave sources \(677\)](#)

1. Introduction

The first and second observing runs of the Advanced LIGO (Abbott et al. 2018) and Virgo (Acernese et al. 2015) gravitational-wave observatories yielded 10 observations of stellar-mass black hole binaries (Abbott et al. 2016a, 2016b), reported in their first gravitational-wave transient catalog (GWTC-1; Abbott et al. 2019a). The question of how these binaries came to merge within the age of the universe remains unanswered. Proposed formation channels typically fall into two categories: *isolated*, in which two stars evolve side-by-side until they form black holes and coalesce (see, e.g., Livio & Soker 1988; Bethe & Brown 1998; de Mink et al. 2010; Ivanova et al. 2013; Kruckow et al. 2016; de Mink & Mandel 2016), and *dynamical*, in which two black holes become bound due to gravitationally driven interactions inside dense star clusters (e.g., Sigurdsson & Hernquist 1993; Portegies Zwart & McMillan 2000; O’Leary et al. 2006; Samsing et al. 2014; Morscher et al. 2015; Fragione & Kocsis 2018; Gondán et al. 2018; Randall & Xianyu 2018a, 2018b; Rodriguez et al. 2018a, 2018b; Samsing 2018; Samsing & D’Orazio 2018; Samsing et al. 2018; Bouffanais et al. 2019; Fragione & Bromberg 2019) and/or active galactic nuclei (AGN) disks (Yang et al. 2019b; Gröbner et al. 2020; McKernan et al. 2020). Young star clusters may create something of a hybrid channel, with dynamical interactions perturbing the evolution of primordial stellar binaries, which evolve to make merging double compact objects (Ziosi et al. 2014; Di Carlo et al. 2019; Rastello et al. 2020).

The component masses and spins of a black hole binary can illuminate its formation history, as can its orbital eccentricity (e.g., Stevenson et al. 2015; Rodriguez et al. 2016; Farr et al. 2017; Fishbach & Holz 2017; Talbot & Thrane 2017; Vitale et al. 2017). Information about these parameters can be extracted from the gravitational-wave signal. Both isolated evolution and dynamical formation can produce black hole binaries with properties like those presented in GWTC-1, with component masses $m_1, m_2 \lesssim 50 M_{\odot}$, dimensionless component spins a_1, a_2 consistent with 0, and eccentricities e consistent with 0 at 10 Hz (Abbott et al. 2019a; Romero-Shaw et al. 2019). Dynamical formation is the preferred pathway for binaries with more extreme masses (Gerosa & Berti 2017; Bouffanais et al. 2019; Rodriguez et al. 2019; Fragione et al. 2020a, 2020b), isotropically distributed spin tilt angles (Rodriguez et al. 2016; Talbot & Thrane 2017), and nonzero orbital eccentricities (Zevin et al. 2017, 2019a; Rodriguez et al. 2018a; Gondán & Kocsis 2019; Samsing et al. 2018).

The mass distribution of black holes that form as the remnants of massive stars is thought to deplete between ~ 50 and $\sim 135 M_{\odot}$ due to pair-instability supernovae (PISN; Heger & Woosley 2002; Özel et al. 2010; Belczynski et al. 2016; Marchant et al. 2016; Fishbach & Holz 2017; Woosley 2017) unless exotic physics is invoked (Sakstein et al. 2020). The precise lower limit of the PISN mass gap is an area of active research; see Belczynski 2020, and references therein. The remnants of binary black hole merger events can have masses within the PISN mass (see, e.g., Abbott et al. 2016a; Fishbach et al. 2017; Chatziioannou et al. 2019; Kimball et al. 2019, 2020). Second-generation mergers—where at least one of the binary components is a remnant of a previous

merger, potentially within the mass gap—can occur in the high-density environments conducive to dynamical mergers (Gerosa & Berti 2017; Bouffanais et al. 2019; Rodriguez et al. 2019; Fragione et al. 2020b). Prior to the detection of GW190521, no convincing evidence has emerged for hierarchical mergers (Fishbach et al. 2017; Abbott et al. 2019b; Chatziioannou et al. 2019; Kimball et al. 2019, 2020).

Isolated binaries are thought to circularize efficiently, leading to negligible eccentricity close to merger (Peters 1964; Hinder et al. 2008). While it is possible that the late-inspiral eccentricity of field mergers can be increased by Kozai–Lidov resonance (Kozai 1962; Lidov 1962) during three-body (Antonini et al. 2017; Fishbach et al. 2017; Silsbee & Tremaine 2017; Rodriguez & Antonini 2018; Liu et al. 2019; Fragione & Kocsis 2020) and four-body (Fragione & Kocsis 2019; Liu & Lai 2019) interactions in the field, the relative rate of such events is expected to be small, assuming moderate progenitor metallicities and black hole natal kicks (Antonini et al. 2017; Silsbee & Tremaine 2017; Rodriguez & Antonini 2018; Liu et al. 2019; Fragione & Kocsis 2020). In contrast, some dynamically formed binaries merge so rapidly after becoming bound that they retain nonnegligible eccentricity in the LIGO–Virgo band (Zevin et al. 2017; Rodriguez et al. 2018b; Samsing et al. 2018; Gondán & Kocsis 2019; Zevin et al. 2019b). Multiple authors (e.g., Samsing & Ramirez-Ruiz 2017; Rodriguez et al. 2018a, 2018b; Samsing 2018; Samsing & D’Orazio 2018) show that we can expect $\mathcal{O}(5\%)$ of all dynamical mergers in globular clusters to have eccentricities $e > 0.1$ at a gravitational-wave frequency of 10 Hz.

The LIGO–Virgo Collaboration (LVC) recently announced the detection of GW190521, a gravitational-wave signal from the merger of a black hole binary with component masses $m_1 = 85_{-14}^{+21} M_\odot$, $m_2 = 66_{-18}^{+17} M_\odot$ (Abbott et al. 2020b, 2020c). The median and 90% confidence intervals quoted for these masses place at least one component within the PISN mass gap.⁵ The data exhibit a modest preference (log Bayes factor $\ln \mathcal{B} \approx 2.4$) for spin-induced precession of the orbital plane, suggesting that the black hole spin vectors may be significantly misaligned from the orbital angular momentum axis. If confirmed, the signature of precession would lend support for the dynamical hypothesis.

In this work, we show that GW190521 is consistent with an eccentric merger. For brevity, we hereafter refer to the eccentricity measured at a gravitational-wave frequency of 10 Hz as e_{10} . Our method allows us to study eccentricities up to $e_{10} = 0.2$, beyond which the waveform is not available. Our analysis reveals overwhelming support for a spin-aligned eccentric signal with $e_{10} \geq 0.1$ over a spin-aligned quasi-circular signal. We use simulated events to demonstrate that precession and eccentricity cannot be distinguished for a GW190521-like signal. We end with a discussion of the implications of our results on the potential formation mechanism of GW190521.

2. Method

We construct eccentric posterior probability density distributions using the method developed in Romero-Shaw et al. (2019), which is built on those introduced by Payne et al. (2019) and Lower et al. (2018). We use the Bayesian inference

⁵ Fishbach & Holz (2020) find that m_1 is above the mass gap if $m_2 < 48 M_\odot$, below the mass gap.

library BILBY (Ashton et al. 2019; Romero-Shaw et al. 2020) to perform an analysis using our “proposal” model: the spin-aligned quasi-circular-waveform model IMRPHENOMD (Khan et al. 2016). We reweight our IMRPHENOMD posteriors to our “target” model: the spin-aligned eccentric waveform SEOBNRE (Cao & Han 2017; Liu et al. 2020). Our prior on eccentricity is log-uniform in the range $-6 \leq \log_{10}(e_{10}) \leq -0.7$. The upper limit arises from waveform limitations, although even a model allowing higher eccentricities would be restricted by the reweighting method. In order to reweight posterior samples efficiently, the samples obtained using the proposal model must cover the same region of the multidimensional parameter space as would be obtained by direct sampling with our target model. The overlap between eccentric and quasi-circular waveforms with otherwise identical parameters falls drastically for higher eccentricities, so their posterior samples would not reside in the same region of the parameter space. We marginalize over the time and phase of coalescence as in Payne et al. (2019) to account for differing definitions of these parameters between our proposal and target models.

3. Analysis of GW190521

We analyze publicly available data and noise power spectral densities from Abbott et al. (2020a, 2020b). We reproduce the settings of the LVC analysis for our parameter estimation, with a data segment of 8 s, a frequency band of 11–512 Hz, and a sampling frequency of 1024 Hz. In order to assess the role of waveform systematics, we perform four analyses using three different waveform models (one waveform is used twice with two different spin priors). The results of these analyses are summarized in Table 1.

First, we analyze the data using the aligned-spin eccentric waveform model SEOBNRE. We present the posterior distribution on the e_{10} of GW190521 in the left panel of Figure 1. The posterior drastically deviates from the log-uniform prior, strongly favoring eccentricities $e_{10} \geq 0.1$. There is little support for $e_{10} < 0.1$, with 90% of the posterior at $e_{10} \geq 0.11$. For other parameters, we obtain median posterior values similar to those given in Table 1 of Abbott et al. (2020b), with a median source-frame total mass $M = 161_{-20}^{+28} M_\odot$, mass ratio $q = 0.7_{-0.3}^{+0.2}$, and $\chi_{\text{eff}} = 0.0_{-0.2}^{+0.2}$. We obtain a luminosity distance, $d_L = 4.0_{-1.7}^{+1.9}$ Gpc, which is slightly lower than (but consistent with) the value of $5.3_{-2.6}^{+2.4}$ Gpc from the LIGO–Virgo analysis. Eccentricity causes a faster merger, reducing the signal power. Thus, in order to match the observed signal-to-noise ratio with an eccentric template, we may require a closer source. Additionally, models like SEOBNRE, IMRPHENOMD, and IMRPHENOMPV2, which do not contain higher-order modes, cannot rule out edge-on binaries, which reduces the median distance estimate (Abbott et al. 2020c). Posterior distribution plots for all other parameters are available online.⁶

Next, we perform an analysis using the precessing waveform IMRPHENOMPV2 (Schmidt et al. 2012) with otherwise identical settings. In Figure 1, we show the posterior distribution for χ_p of GW190521 obtained with IMRPHENOMPV2. This analysis recovers a smaller median d_L than the SEOBNRE analysis, with a more extreme mass ratio, $q \approx 0.5$. In order to carry out model selection comparing the IMRPHENOMPV2 results to those obtained with SEOBNRE, we

⁶ git.ligo.org/isobel.romero-shaw/gw190521.1

Table 1

Recovered GW190521 Parameter Values Obtained Using Eccentric Waveform Model SEOBNRE, Precessing Waveform Models IMRPHENOMPV2 and NRSUR7DQ4, and NRSUR7DQ4 Constrained to have Aligned Spins

Parameter (Source Frame)	SEOBNRE	IMRPHENOMPV2	NRSUR7DQ4	NRSUR7DQ4 Aligned	NRSUR7DQ4 LVC
Primary mass, $m_1 [M_\odot]$	92^{+26}_{-16}	126^{+61}_{-41}	86^{+18}_{-13}	85^{+22}_{-14}	85^{+21}_{-14}
Secondary mass, $m_2 [M_\odot]$	69^{+18}_{-19}	59^{+32}_{-24}	69^{+18}_{-17}	61^{+15}_{-17}	66^{+17}_{-18}
Luminosity distance, d_L [Gpc]	$4.1^{+1.8}_{-1.8}$	$2.4^{+2.3}_{-1.0}$	$4.7^{+2.2}_{-2.2}$	$4.7^{+1.6}_{-1.5}$	$5.3^{+2.4}_{-2.6}$
Right ascension, α [rad]	$3.6^{+2.7}_{-3.5}$	$4.3^{+1.9}_{-4.3}$	$3.4^{+2.9}_{-3.4}$	$3.7^{+2.6}_{-3.7}$	$3.5^{+2.8}_{-3.4}$
decl., δ [rad]	$-0.7^{+1.4}_{-0.5}$	$-0.7^{+1.5}_{-0.4}$	$-0.8^{+1.5}_{-0.4}$	$-0.9^{+1.6}_{-0.3}$	$-0.8^{+1.5}_{-0.4}$
Reference phase, ϕ [rad]	$3.1^{+2.9}_{-2.7}$	$3.0^{+3.0}_{-2.7}$	$3.2^{+2.6}_{-2.6}$	$3.1^{+2.9}_{-2.8}$	$3.4^{+2.6}_{-3.2}$
Polarization, ψ [rad]	$1.5^{+1.5}_{-1.4}$	$1.6^{+1.3}_{-1.5}$	$1.8^{+1.2}_{-1.5}$	$1.6^{+1.4}_{-1.4}$	$1.8^{+1.2}_{-1.6}$
Inclination, θ_{JN} [rad]	$1.3^{+1.6}_{-1.0}$	$1.4^{+1.0}_{-0.7}$	$0.8^{+2.0}_{-0.6}$	$0.7^{+2.2}_{-0.5}$	$0.8^{+2.1}_{-0.6}$
Eccentricity lower limit at 10 Hz, e_{10}^{\min}	0.11	N/A	N/A	N/A	N/A
Effective spin, χ_{eff}	$0.0^{+0.2}_{-0.2}$	$0.1^{+0.4}_{-0.4}$	$0.0^{+0.3}_{-0.3}$	$0.0^{+0.2}_{-0.3}$	$0.1^{+0.3}_{-0.4}$
Effective precession, χ_p	N/A	$0.7^{+0.2}_{-0.3}$	$0.6^{+0.2}_{-0.3}$	N/A	$0.7^{+0.3}_{-0.4}$
Log Bayes factor against SEOBNRE, $\ln \mathcal{B}_{X/E}$	0.0	-2.0	-1.8	-5.0	-1.2

Note. For the SEOBNRE analysis, we give the 90% confidence lower limit on eccentricity at 10 Hz. For other parameters, the median of the posterior is given along with the 90% credible interval. In the final column, we state the values inferred from the LIGO–Virgo analysis, read from the public posterior samples obtained using NRSUR7DQ4 (Abbott et al. 2020a). In the final row, we provide the log Bayes factor of each analysis against the signal-to-noise log Bayes factor obtained for $e_{10} \geq 0.1$ using SEOBNRE ($\ln \mathcal{B}_{S/N} = 85.7$).

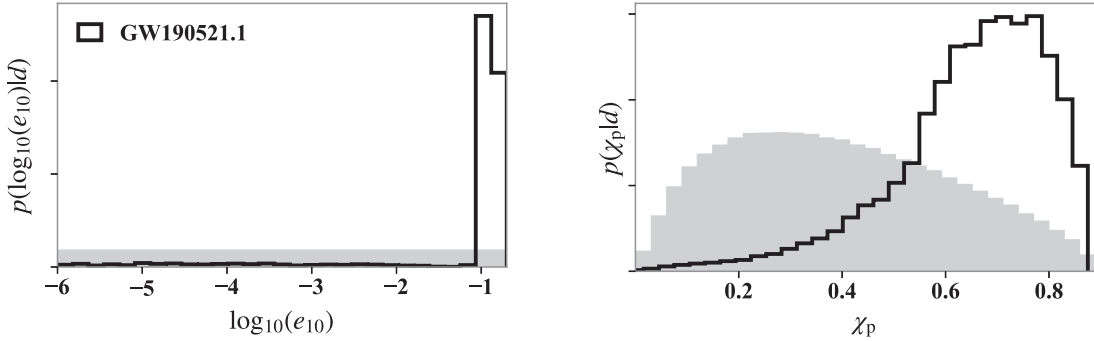


Figure 1. Results of analysis of GW190521 using SEOBNRE and IMRPHENOMPV2. Left: posterior probability density distribution for eccentricity at 10 Hz for GW190521, recovered using SEOBNRE. At 90% confidence, $e_{10} \geq 0.11$. The posterior rails against the upper limit of the prior, $e_{10} = 0.2$, suggesting that the true value lies beyond this waveform-enforced constraint. Right: posterior probability density distribution for the precession parameter χ_p for GW190521, recovered using IMRPHENOMPV2. The prior probability for each parameter is shown in gray.

implement an astrophysically motivated prior on eccentricity. Theoretical studies robustly predict that $\sim 5\%$ of binaries that form dynamically in globular clusters will have $e_{10} \geq 0.1$ (e.g., Rodriguez et al. 2018b; Samsing 2018; Samsing et al. 2018; Kremer et al. 2020). To investigate this hypothesis, we assume a log-uniform distribution for $\log_{10} e_{10} \in (-1, -0.7)$. Using this astrophysically motivated prior, the eccentric model is mildly preferred to the precessing model by a factor of $\ln \mathcal{B}_{E/P} = 2.0$. If we repeat the same calculation using the (less well-motivated) prior range $\log_{10} e_{10} \in (-6, -0.7)$ as in Figure 1, the eccentric (E) and precessing (P) waveform models are almost equally well-supported by the data, with a log Bayes factor $\ln \mathcal{B}_{E/P} = -0.35$.

Finally, we perform computationally intensive analyses using the precessing, higher-order-model waveform NRSUR7DQ4, using parallel BILBY (Smith et al. 2020) to manage computational costs. We run two versions of the NRSUR7DQ4 analysis: one assuming aligned black hole spins (no precession) and one allowing arbitrary spin orientations (allowing precession). Otherwise, the assumptions are identical to the IMRPHENOMPV2 analysis above. While the two NRSUR7DQ4 analyses obtain near-identical results, the analysis that includes precession (P) is preferred over the no-precession

hypothesis with a moderate $\ln \mathcal{B}_{P/NP} = 3.2$. The eccentric SEOBNRE hypothesis (with $e_{10} > 0.1$) is preferred to the precessing and nonprecessing NRSUR7DQ4 analyses by log Bayes factors of $\ln \mathcal{B}_{E/P} = 1.8$ and $\ln \mathcal{B}_{E/NP} = 5.0$, respectively.

We perform two additional analyses, identical in almost all aspects to the NRSUR7DQ4 studies described above, but without including higher-order modes. If we assume aligned spin, we obtain results similar to the SEOBNRE analysis. If we allow for precession, we obtain results similar to the IMRPHENOMPV2 results with luminosity distance $2.8^{+2.2}_{-1.5}$ Gpc (90% credibility) and $q \approx 0.5$.

4. Injection Studies

Ideally, one would analyze gravitational-wave signals using models that include both precession and eccentricity. This would allow simultaneous measurements of χ_p and e_{10} , as well as illuminating the full extent of the degeneracy between the two parameters and how that degeneracy changes with mass. Unfortunately, such models do not yet exist; see Healy et al. (2009) and Levin et al. (2011) for a theoretical background of eccentric and precessing binary dynamics and waveforms. Thus, we use numerical tests to explore how our limited

Table 2

The 90% Credible Upper Limit on Eccentricity at 10 Hz, e_{10}^{\max} , and Recovered Precession Parameter χ_p for Different Injections with Varying Waveform Model, e_{10} and χ_p Settings

Injected Waveform Model	Injected e_{10}	Injected χ_p	Recovered e_{10}^{\max} with SEOBNRE	Recovered χ_p with IMRPHENOMPV2
IMRPHENOMD	0	0	0.025	$0.39^{+0.37}_{-0.29}$
NRSUR7DQ4	0	0	0.032	$0.33^{+0.40}_{-0.25}$
SEOBNRE	0	0	0.055	$0.42^{+0.36}_{-0.30}$
IMRPHENOMPV2	0	0.63	0.077	$0.43^{+0.35}_{-0.32}$
NRSUR7DQ4	0	0.63	0.118	$0.53^{+0.29}_{-0.37}$
SEOBNRE	0.13	0	0.136	$0.57^{+0.26}_{-0.39}$

Note. For the recovered χ_p we quote the posterior median and 90% credible interval.

waveform models affect what we infer about eccentricity and precession. We generate six GW190521-like waveform templates using different waveform models, each with different values of e_{10} and χ_p ; see Table 2. Other parameters are identical to those in Table 3. Using BILBY, we inject these waveforms into simulated detector networks consisting of LIGO Hanford, LIGO Livingston, and Virgo, with noise power spectral densities matching those used for analysis of GW190521 (Abbott et al. 2020b). For each injection, we recover the signal using both the aligned-spin eccentric model SEOBNRE and the quasi-circular precessing model IMRPHENOMPV2.

In Figure 2, we compare the posterior distributions for e_{10} (obtained using SEOBNRE) and χ_p (obtained using IMRPHENOMPV2) for all injections. When circular, nonprecessing waveforms are injected, the SEOBNRE analysis recovers posterior distributions for e_{10} consistent with the prior below the 90% credible upper limit, $e_{10}^{\max} \leq 0.025$ (0.032, 0.055) for injected IMRPHENOMD (NRSUR7DQ4, SEOBNRE) waveforms. For these same waveforms, IMRPHENOMPV2 analysis recovers posteriors consistent with the prior on χ_p . When we increase only χ_p , the posteriors on both χ_p and e_{10} skew away from their priors. This is most notable for the NRSUR7DQ4 injections, suggesting that higher-order modes (included in NRSUR7DQ4, but not in IMRPHENOMPV2) may be important for distinguishing precession and eccentricity. When we increase e_{10} , both posteriors deviate from their priors, more significantly than for the increased-precession case. These injection studies demonstrate that, for GW190521-like binaries, precession may be mistaken for eccentricity, and that the imprint of eccentricity may be mistaken for that of precession. We provide the full posterior distributions for all parameters in these injection studies online.⁷

5. Discussion

Assuming the aligned-spin SEOBNRE waveform model, we infer an eccentricity $e_{10} \gtrsim 0.1$ for GW190521. We find that the SEOBNRE waveform is slightly preferred over the circular-waveform models NRSUR7DQ4 and IMRPHENOMPV2, both of which allow for precession. While we lack a waveform model that can simultaneously account for precession and eccentricity, GW190521 could be later verified as the first detection of a binary black hole with $e_{10} \geq 0.1$. The presence of either precession or eccentricity adds weight to the hypothesis that the progenitor of GW190521 formed dynamically.

Table 3

Parameters Shared by All Injected Waveforms

Parameter (Source Frame)	Value
Primary mass, $m_1 [M_\odot]$	84
Secondary mass, $m_2 [M_\odot]$	62
Luminosity distance, d_L [Gpc]	5.0
R.A., α [rad]	3.3
Decl., δ [rad]	0.5
Reference phase, ϕ [rad]	6.2
Polarization, ψ [rad]	1.6
Inclination, θ_{JN} [rad]	0.3
Geocent time, t_0 [s]	1242442967.46

Samsing (2018) predicts there are ~ 19 dynamical mergers with $e_{10} < 0.1$ for every merger with $e_{10} \geq 0.1$ —a prediction thought to be robust to details about the globular cluster model; see also Rodriguez et al. (2018b) and Martinez et al. (2020). From the public alerts listed on GraceDB,⁸ there are $\mathcal{O}(30)$ binary black hole mergers from the first half of LIGO–Virgo’s third observing run (O3a). Combining these with the results of Abbott et al. (2019a), Venumadhav et al. (2019, 2020), and Zackay et al. (2019), the total number of binary black holes observed in gravitational waves is $\mathcal{O}(50)$. If globular cluster mergers dominate LIGO and Virgo’s observed black hole mergers, we expect $2.5^{+2.0}_{-2.5}$ mergers with $e_{10} \geq 0.1$ from the first 50 binary black hole observations. Thus, it would not be surprising if GW190521 is determined to be highly eccentric. Moreover, if GW190521 is eccentric, then O3a may provide us with another $1.5^{+2.0}_{-1.5}$ event with $e_{10} \geq 0.1$, assuming that O3a searches did not miss them; the signals of highly eccentric binaries may be missed by compact binary coalescence (CBC) and burst searches (East et al. 2013).

We note that while GW190521 may have formed within a globular cluster, this is not its only viable formation pathway. Dynamical formation may also occur in active galactic nuclei (e.g., Kocsis & Levin 2012; Yang et al. 2019a; Gröbner et al. 2020), nuclear star clusters (e.g., Mapelli et al. 2020), young open clusters (e.g., Di Carlo et al. 2019), and young massive clusters (Banerjee 2017, 2018a, 2018b, 2020; Kremer et al. 2020). Mergers in young star clusters are likely to take place after ejection, giving the binary ample time to circularize and making young star clusters a less promising explanation for eccentric binaries. Both active galactic nuclei and globular clusters may produce binary black holes with misaligned spin and/or eccentricity, and so it is not clear which dynamical

⁷ git.ligo.org/isobel.romero-shaw/gw190521.1/injection_studies

⁸ gracedb.ligo.org/superevents/public/O3/

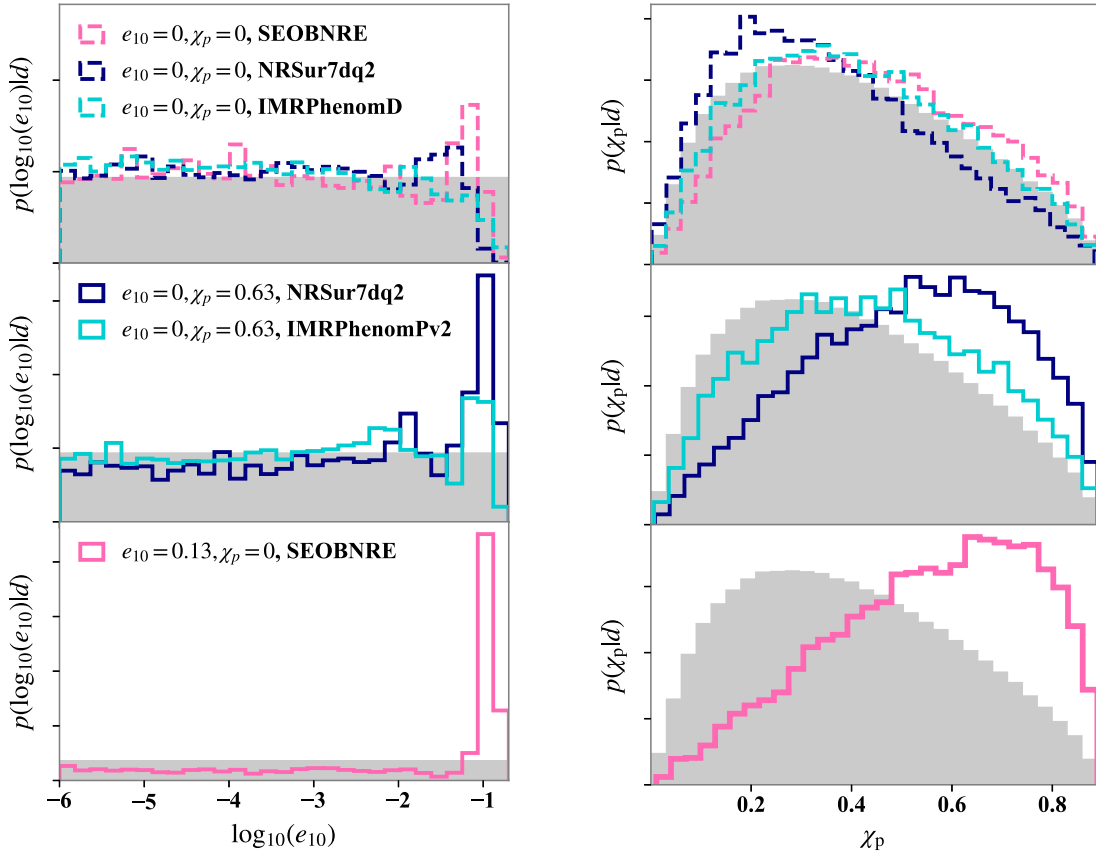


Figure 2. Results of SEOBNRE and IMRPHENOMPv2 analysis of simulated data using GW190521-like injections. Left: posterior distributions for eccentricity at 10 Hz for GW190521-like injection studies with varying e_{10} and χ_p , obtained using SEOBNRE. Right: posterior distribution for precession parameter χ_p for GW190521-like injection studies with varying e_{10} and χ_p , recovered using IMRPHENOMPv2. The prior distributions are shown in gray.

formation pathway is favored for GW190521. Regardless, both precession and eccentricity are signatures of dynamical formation; therefore, GW190521 is likely to have formed in a dense stellar environment conducive to dynamical interactions.

In dense environments like those mentioned above, binary black hole merger remnants may have masses within the mass gap. If these mergers are retained within the cluster, then they may merge again, producing intermediate-mass black holes. As an alternative to hierarchical black hole mergers, Roupas & Kazanas (2019) argue that black holes may accrete enough gas in protoclusters to enter into the mass gap. Another option is the direct collapse of stellar merger remnants to mass gap black holes (e.g., Spera et al. 2019; Kremer et al. 2020). These black holes may undergo subsequent dynamical mergers if their environments are sufficiently densely populated. Although the high masses of GW190521 render it incompatible with current models of isolated binary evolution, these masses can be produced in models where various model assumptions are substantially relaxed (see, e.g., Farmer et al. 2019; Stevenson et al. 2019; Marchant & Moriya 2020).

For GW190521-like signals, we highlight the degeneracy between eccentricity and precession.⁹ This complements the results of Bustillo et al. (2020), who found that for the gravitational-wave signal of a head-on black hole collision ($e_{10} = 1$) with total mass in the range $M \in (130, 300)M_{\odot}$ can





⁹ The degeneracy between eccentricity and precession is less pronounced for less massive systems, which have longer signals in-band.

be indistinguishable from the signal of a much more distant quasi-circular precessing binary. Recently, a candidate electromagnetic counterpart for GW190521 was observed at ≈ 2.8 Gpc and reported by Graham et al. (2020), who propose that a binary black hole merger in an AGN disk might have such a counterpart. Extrapolating between the $e_{10} = 1$ results from Bustillo et al. (2020) and the results shown here, the detected distance of GW190521 in gravitational waves is consistent with the electromagnetic counterpart if GW190521 had an eccentricity in the range $0.2 < e_{10} < 1.0$, a region of parameter space that cannot be fully explored with existing gravitational waveform models. However, new developments in eccentric waveforms (see, e.g., Chiaramello & Nagar 2020) may allow us to start probing previously unexplored parameter space in the near future. If the transient reported by Graham et al. (2020) is truly an electromagnetic counterpart emanating from an AGN disk merger, it would be consistent with the hypothesis that GW190521 was an eccentric binary, since orbital eccentricity vastly increases the merger rate from such environments; see Gröbner et al. (2020).

We thank the anonymous referee for their thoughtful suggestions, which improved the manuscript. We thank Colm Talbot, Max Isi, Alan Weinstein, Tito Dal Canton, Christopher Berry, and Chase Kimball for fruitful suggestions and illuminating discussions. We thank Rory Smith for assistance with parallel BILBY. This work is supported through Australian Research Council (ARC) Future Fellowships FT150100281, FT160100112, Centre of Excellence CE170100004, and

Discovery Project DP180103155. J.C.B. acknowledges support from the Direct Grant of the CUHK Research Committee, Project ID: 4053406. J.C.B. also received the support of a fellowship from “la Caixa” Foundation (ID 100010434) and from the European Union’s Horizon 2020 research and innovation programme under the Marie Skłodowska-Curie grant agreement No 847648, fellowship code LCF/BQ/PI20/11760016. Computing was performed on the OzSTAR Australian national facility at Swinburne University of Technology, which receives funding in part from the Astronomy National Collaborative Research Infrastructure Strategy (NCRIS) allocation provided by the Australian Government, and the LIGO Laboratory computing cluster at California Institute of Technology, supported by National Science Foundation Grants PHY-0757058 and PHY-0823459. LIGO was constructed by the California Institute of Technology and Massachusetts Institute of Technology with funding from the National Science Foundation and operates under cooperative agreement PHY-1764464. Virgo is funded by the French Centre National de Recherche Scientifique (CNRS), the Italian Istituto Nazionale della Fisica Nucleare (INFN) and the Dutch Nikhef, with contributions by Polish and Hungarian institutes. During the final stages of preparation of this manuscript, we became aware of the work of Gayathri et al. (2020), who compare numerical-relativity waveform simulations to GW190521. Numerical-relativity waveforms are too computationally expensive to be used for Bayesian parameter estimation. However, the fact that Gayathri et al. (2020) find that eccentric numerical-relativity simulations are consistent with GW190521 supports the conclusions drawn in our work.

ORCID iDs

Isobel Romero-Shaw  <https://orcid.org/0000-0002-4181-8090>
 Paul D. Lasky  <https://orcid.org/0000-0003-3763-1386>
 Eric Thrane  <https://orcid.org/0000-0002-4418-3895>
 Juan Calderón Bustillo  <https://orcid.org/0000-0002-4171-5884>

References

- Abbott, B. P., Abbott, R., Abbott, T. D., et al. 2016a, *PhRvL*, **116**, 061102
 Abbott, B. P., Abbott, R., Abbott, T. D., et al. 2016b, *PhRvX*, **6**, 041015
 Abbott, B. P., Abbott, R., Abbott, T. D., et al. 2018, *LRR*, **21**, 3
 Abbott, B. P., Abbott, R., Abbott, T. D., et al. 2019a, *PhRvX*, **9**, 031040
 Abbott, B. P., Abbott, R., Abbott, T. D., et al. 2019b, *ApJ*, **883**, 149
 Abbott, B. P., Abbott, R., Abbott, T. D., et al. 2020a, Gravitational Wave Open Science Center Strain Data Release for GW190521, LIGO Open Science Center, https://www.gw-openscience.org/eventapi/html/O3_Discovery_Papers/GW190521/v2/
 Abbott, R., Abbott, T. D., Abraham, S., et al. 2020b, *PhRvL*, **125**, 101102
 Abbott, R., Abbott, T. D., Abraham, S., et al. 2020c, *ApJL*, **900**, L13
 Acernese, F., Agathos, M., Agatsuma, K., et al. 2015, *CQGra*, **32**, 024001
 Antonini, F., Toonen, S., & Hamers, A. S. 2017, *ApJ*, **841**, 77
 Ashton, G., Hübner, M., Lasky, P. D., et al. 2019, *ApJS*, **241**, 27
 Banerjee, S. 2017, *MNRAS*, **467**, 524
 Banerjee, S. 2018a, *MNRAS*, **473**, 909
 Banerjee, S. 2018b, *MNRAS*, **481**, 5123
 Banerjee, S. 2020, *MNRAS*, in press (doi:10.1093/mnras/staa2392)
 Belczynski, K. 2020, arXiv:2009.13526
 Belczynski, K., Heger, A., Gladysz, W., et al. 2016, *A&A*, **594**, A97
 Bethe, H. A., & Brown, G. E. 1998, *ApJ*, **506**, 780
 Bouffanais, Y., Mapelli, M., Gerosa, D., et al. 2019, *ApJ*, **886**, 25
 Bustillo, J. C., Sanchis-Gual, N., Torres-Forné, A., & Font, J. A. 2020, arXiv:2009.01066
 Cao, Z., & Han, W.-B. 2017, *PhRvD*, **96**, 044028
 Chatziioannou, K., Cotesta, R., Sudarshan, G., et al. 2019, *PhRvD*, **100**, 104015
 Chiamarello, D., & Nagar, A. 2020, *PhRvD*, **101**, 101501
 de Mink, S. E., & Mandel, I. 2016, *MNRAS*, **460**, 3545
 de Mink, S. E., Cantiello, M., Langer, N., & Pols, O. R. 2010, in AIP Conf. Proc. 1314, International Conference on Binaries: In Celebration of Ron Webbink’s 65th Birthday, ed. V. Kalogera & M. van der Sluys (Melville, NY: AIP), 291
 Di Carlo, U. N., Giacobbo, N., Mapelli, M., et al. 2019, *MNRAS*, **487**, 2947
 East, W. E., McWilliams, S. T., Levin, J., & Pretorius, F. 2013, *PhRvD*, **87**, 043004
 Farmer, R., Renzo, M., de Mink, S. E., Marchant, P., & Justham, S. 2019, *ApJ*, **887**, 53
 Farr, W. M., Stevenson, S., Coleman, M., et al. 2017, *Natur*, **548**, 426
 Fishbach, M., & Holz, D. E. 2017, *ApJL*, **851**, L25
 Fishbach, M., & Holz, D. E. 2020, arXiv:2009.05472
 Fishbach, M., Holz, D. E., & Farr, B. 2017, *ApJL*, **840**, L24
 Fragione, G., & Bromberg, O. 2019, *MNRAS*, **488**, 4370
 Fragione, G., & Kocsis, B. 2018, *PhRvL*, **121**, 161103
 Fragione, G., & Kocsis, B. 2019, *MNRAS*, **486**, 4781
 Fragione, G., & Kocsis, B. 2020, *MNRAS*, **493**, 3920
 Fragione, G., Loeb, A., & Rasio, F. A. 2020a, *ApJL*, **902**, L26
 Fragione, G., Loeb, A., & Rasio, F. A. 2020b, *ApJL*, **895**, L15
 Gayathri, V., Healy, J., Lange, J., et al. 2020, arXiv:2009.05461
 Gerosa, D., & Berti, E. 2017, *PhRvD*, **95**, 124046
 Gondán, L., & Kocsis, B. 2019, *ApJ*, **871**, 178
 Gondán, L., Kocsis, B., Raffai, P., & Frei, Z. 2018, *ApJ*, **860**, 5
 Graham, M. J., Ford, K. E. S., McKernan, B., et al. 2020, *PhRvL*, **124**, 251102
 Gröbner, M., Ishibashi, W., Tiwari, S., Haney, M., & Jetzer, P. 2020, *A&A*, **638**, A119
 Healy, J., Levin, J., & Shoemaker, D. 2009, *PhRvL*, **103**, 131101
 Heger, A., & Woosley, S. E. 2002, *ApJ*, **567**, 532
 Hinder, I., Vaishnav, B., Hermann, F., Shoemaker, D. M., & Laguna, P. 2008, *PhRvD*, **77**, 081502
 Ivanova, N., Justham, S., Chen, X., et al. 2013, *A&ARv*, **21**, 59
 Khan, S., Husa, S., Hannam, M., et al. 2016, *PhRvD*, **93**, 044007
 Kimball, C., Berry, C., & Kalogera, V. 2019, *RNAAS*, **4**, 2
 Kimball, C., Talbot, C., Berry, C.P. L., et al. 2020, *ApJ*, **900**, 177
 Kocsis, B., & Levin, J. 2012, *PhRvD*, **85**, 123005
 Kozai, Y. 1962, *ApJ*, **67**, 591
 Kremer, K., Spera, M., Becker, D., et al. 2020, arXiv:2006.10771
 Kruckow, M. U., et al. 2016, *A&A*, **596**, A58
 Levin, J., McWilliams, S. T., & Contreras, H. 2011, *CQGra*, **28**, 175001
 Lidov, M. L. 1962, *P&SS*, **9**, 719
 Liu, B., & Lai, D. 2019, *MNRAS*, **483**, 4060
 Liu, B., Lai, D., & Wang, Y.-H. 2019, *ApJ*, **881**, 41
 Liu, X., Cao, Z., & Shao, L. 2020, *PhRvD*, **101**, 044049
 Livio, M., & Soker, N. 1988, *ApJ*, **329**, 764
 Lower, M., Thrane, E., Lasky, P. D., & Smith, R. 2018, *PhRvD*, **98**, 083028
 Mapelli, M., Santoliquido, F., Bouffanais, Y., et al. 2020, arXiv:2007.15022
 Marchant, P., Langer, N., Podsiadlowski, P., Tauris, T. M., & Moriya, T. J. 2016, *A&A*, **588**, A50
 Marchant, P., & Moriya, T. 2020, *A&A*, **640**, L18
 Martinez, M. A. S., Fragione, G., Kremer, K., et al. 2020, arXiv:2009.08468
 McKernan, B., Ford, K. E. S., & O’Shaughnessy, R. 2020, *MNRAS*, **498**, 4088
 Morscher, M., Pattabiraman, B., Rodriguez, C., Rasio, F. A., & Umbreit, S. 2015, *ApJ*, **800**, 9
 O’Leary, R. M., Rasio, F. A., Fregeau, J. M., Ivanova, N., & O’Shaughnessy, R. 2006, *ApJ*, **637**, 937
 Özel, F., Psaltis, D., Narayan, R., & McClintock, J. E. 2010, *ApJ*, **725**, 1918
 Payne, E., Talbot, C., & Thrane, E. 2019, *PhRvD*, **100**, 123017
 Peters, P. C. 1964, *PhRv*, **136**, B1224
 Portegies Zwart, S. F., & McMillan, S. 2000, *ApJL*, **528**, L17
 Randall, L., & Xianyu, Z.-Z. 2018a, *ApJ*, **853**, 93
 Randall, L., & Xianyu, Z.-Z. 2018b, *ApJ*, **864**, 134
 Rastello, S., Mapelli, M., Di Carlo, U. N., et al. 2020, *MNRAS*, **497**, 1563
 Rodriguez, C. L., & Antonini, F. 2018, *ApJ*, **863**, 7
 Rodriguez, C. L., Amaro-Seoane, P., Chatterjee, S., et al. 2018a, *PhRvD*, **98**, 123005
 Rodriguez, C. L., Amaro-Seoane, P., Chatterjee, S., & Rasio, F. A. 2018b, *PhRvL*, **120**, 151101
 Rodriguez, C. L., Zevin, M., Amaro-Seoane, P., et al. 2019, *PhRvD*, **100**, 043027

- Rodriguez, C. L., Zevin, M., Pankow, C., Kalogera, V., & Rasio, F. A. 2016, *ApJL*, **832**, L2
- Romero-Shaw, I. M., Lasky, P. D., & Thrane, E. 2019, *MNRAS*, **490**, 5210
- Romero-Shaw, I. M., Talbot, C., Biscoveanu, S., et al. 2020, *MNRAS*, in press (doi:10.1093/mnras/staa2850)
- Roupas, Z., & Kazanas, D. 2019, *A&A*, **632**, L8
- Sakstein, J., Croon, D., McDermott, S. D., Straight, M. C., & Baxter, E. J. 2020, arXiv:2009.01213
- Samsing, J. 2018, *PhRvD*, **D97**, 103014
- Samsing, J., & D’Orazio, D. J. 2018, *MNRAS*, **481**, 5445
- Samsing, J., D’Orazio, D. J., Askar, A., & Gierz, M. 2018, arXiv:1802.08654
- Samsing, J., MacLeod, M., & Ramirez-Ruiz, E. 2014, *ApJ*, **784**, 71
- Samsing, J., & Ramirez-Ruiz, E. 2017, *ApJL*, **840**, L14
- Schmidt, P., Hannam, M., & Husa, S. 2012, *PhRvD*, **86**, 104063
- Sigurdsson, S., & Hernquist, L. 1993, *Natur*, **364**, 423
- Silsbee, K., & Tremaine, S. 2017, *ApJ*, **836**, 39
- Smith, R., Ashton, G., Vajpeyi, A., & Talbot, C. 2020, *MNRAS*, **498**, 4492
- Spera, M., Mapelli, M., Giacobbo, N., et al. 2019, *MNRAS*, **485**, 889
- Stevenson, S., Ohme, F., & Fairquist, S. 2015, *ApJ*, **810**, 58
- Stevenson, S., Sampson, M., Powell, J., et al. 2019, *ApJ*, **882**, 121
- Talbot, C., & Thrane, E. 2017, *PhRvD*, **96**, 023012
- Venumadhav, T., Zackay, B., Roulet, J., Dai, L., & Zaldarriaga, M. 2020, *PhRvD*, **101**, 083030
- Venumadhav, T., Zackay, B., Roulet, J., Dai, L., & Zaldarriaga, M. 2019, *PhRvD*, **100**, 023011
- Vitale, S., Lynch, R., Sturani, R., & Graff, P. 2017, *CQGra*, **34**, 03LT01
- Woosley, S. E. 2017, *ApJ*, **836**, 244
- Yang, Y., Bartos, I., Gayathri, V., et al. 2019a, *PhRvL*, **123**, 181101
- Yang, Y., Bartos, I., Haiman, Z., et al. 2019b, *ApJ*, **876**, 122
- Zackay, B., Dai, L., Venumadhav, T., Roulet, J., & Zaldarriaga, M. 2019, arXiv:1910.09528
- Zevin, M., Kremer, K., Siegel, D. M., et al. 2019b, *ApJ*, **886**, 4
- Zevin, M., Pankow, C., Rodriguez, C. L., et al. 2017, *ApJ*, **846**, 82
- Zevin, M., Samsing, J., Rodriguez, C., et al. 2019a, *ApJ*, **871**, 91
- Ziosi, B. M., Mapelli, M., Branchesi, M., & Tormen, G. 2014, *MNRAS*, **441**, 3703